

Article

Hydrological Connectivity Response of Typical Soil and Water Conservation Measures Based on SIMulated Water Erosion Model: A Case Study of Tongshuang Watershed in the Black Soil Region of Northeast China

Muzi Li ^{1,2}, Bin Wang ^{1,2,*} , Wengang Wang ^{1,2}, Zuming Chen ¹ and Shenyao Luo ¹

¹ School of Soil and Water Conservation, Beijing Forestry University, Beijing 100083, China; chengyu2004@163.com (M.L.); w13279357926@163.com (W.W.); chenzm14@gmail.com (Z.C.); 19079567638@163.com (S.L.)

² Three-Gorges Area (Chongqing) Jinyun Forest Eco-System Research Station, Beijing 100083, China

* Correspondence: wangbin1836@bjfu.edu.cn

Abstract: The black soil region of Northeast China is the largest commercial grain production base in China, accounting for about 25% of the total in China. In this region, the water erosion is prominent, which seriously threatens China's food security. It is of great significance to effectively identify the erosion-prone points for the prevention and control of soil erosion on the slope of the black soil region in Northeast China. This article takes the Tongshuang small watershed (Heilongjiang Province in China) as an example, which is dominated by hilly landforms with mainly black soil and terraces planted with corn and soybeans. Based on the 2.5 cm resolution Digital Elevation Model (DEM) reconstructed by unmanned aerial vehicles (UAVs), we explore the optimal resolution for hydrological simulation research on sloping farmland in the black soil region of Northeast China and explore the critical water depth at which erosion damage occurs in ridges on this basis. The results show that the following: (1) Compared with the 2 m resolution DEM, the interpretation accuracy of field roads, wasteland, damaged points, ridges and cultivated land at the 0.2 m resolution is increased by 4.55–27.94%, which is the best resolution in the study region. (2) When the water depth is between 0.335 and 0.359 m, there is a potential erosion risk of ridges. When the average water depth per unit length is between 0.0040 and 0.0045, the ridge is in the critical range for its breaking, and when the average water depth per unit length is less than the critical range, ridge erosion damage occurs. (3) When local erosion damage occurs, the connectivity will change abruptly, and the remarkable change in the index of connectivity (IC) can provide a reference for predicting erosion damage.

Keywords: soil erosion; SIMWE; high-resolution terrain; Northeast Black Soil Region



Citation: Li, M.; Wang, B.; Wang, W.; Chen, Z.; Luo, S. Hydrological Connectivity Response of Typical Soil and Water Conservation Measures Based on SIMulated Water Erosion Model: A Case Study of Tongshuang Watershed in the Black Soil Region of Northeast China. *Water* **2024**, *16*, 2568. <https://doi.org/10.3390/w16182568>

Academic Editors: Jay Jabro and Catherine N. Mulligan

Received: 4 June 2024

Revised: 26 August 2024

Accepted: 3 September 2024

Published: 10 September 2024



Copyright: © 2024 by the authors. Licensee MDPI, Basel, Switzerland. This article is an open access article distributed under the terms and conditions of the Creative Commons Attribution (CC BY) license (<https://creativecommons.org/licenses/by/4.0/>).

1. Introduction

Soil erosion is a prominent environmental problem in the world which seriously restricts the survival and development of human beings, and it has become a common concern in the world [1]. Soil erosion can lead to land degradation and reduced soil fertility, affecting national food security and economic development [2–4]. Black soil has good physical properties and is fertile, and is it known as the “giant panda in cultivated land”. Globally, black soil is mainly concentrated in four black soil regions: the Mississippi Plain, the Ukrainian Plain, the Northeast China Plain and the Pampas, accounting for about one-sixth of the world's arable land. The black soil region of Northeast China is the largest commercial grain production base in China, accounting for about 25% of the total in China. The total area of black soil in China is about 1.0876 million km². Due to high-intensity development and utilization, the black soil layer is eroded, the soil structure is damaged, and serious degradation occurs. According to the dynamic monitoring results

of soil erosion by the Chinese Authorities, the eroded surface of these soils in China was 208,900 km² in 2023. From the middle of the last century to the present, the thickness of the black soil layer has decreased by about 40 cm and the average annual loss of black soil is 0.1–0.5 cm. The annual grain yield has reduced by as high as 14.7%, posing a serious threat to food security and ecological security [5].

The black soil region of Northeast China is located in the middle and high latitudes of China and has a cold temperate continental monsoon climate [6]. The types of erosion include water erosion, wind erosion, and freeze–thaw erosion, among which water erosion is the main erosion type. In 2023, the area affected by water erosion was 133,200 km², accounting for 12.25% of the total area of the black soil region. In the black soil region of Northeast China, the main tillage methods are alternate ridges and beds, which are more prone to surface runoff and soil erosion than other ridge tillage methods due to the confluence effect of ridge tillage [7]. In recent years, the popularization and application of terraces has played an obvious role in water storage and soil conservation, which can effectively reduce the impact of soil erosion on agricultural production by reducing slope and slope length, changing hydrological processes, and reducing hydrological connectivity [8]. However, unreasonable terraced designs can cause runoff accumulation and local instability, leading to terrace collapse and damage and exacerbating soil erosion [9,10]. Existing research mostly simulates the outdoor environment through indoor soil channel erosion experiments [11,12], while traditional simulation experiments cannot accurately reflect the characteristics of complex underlying surfaces in the field. Moreover, the experimental operation is difficult, and the corresponding conditions of the results are singular. It is of great significance for the prevention and control of soil erosion on slopes to accurately reflect the characteristics of surface micro-topography with the help of a distributed hydrological model, effectively identify erosion-prone points, and deepen the understanding of slope hydrological processes.

The Digital Elevation Model (DEM) is the basis of hydrological simulation analysis, and the resolution of these models has an important impact on the extraction of hydrological analysis parameters, which in turn affects the simulation accuracy of the model. In general, the higher the spatial resolution of the DEM, the more accurately it can reflect the condition of the underlying surface and the better the simulation results of the hydrological model. Low-resolution DEM terrain features are prone to loss, resulting in large deviations in hydrological calculation and analysis, which cannot meet the requirements of relevant applications [13]. With technological advances, hydrological distribution models can more comprehensively consider the spatial variability of land surface factors and improve the accuracy of simulations, and they have been widely used in soil erosion research [14].

The SIMulated Water Erosion model (SIMWE) developed based on the theoretical framework of the Water Erosion Prediction Project model (WEPP) can better describe the water flow path and the spatial distribution of erosion and sedimentation under complex terrain conditions, which is sensitive to the change in DEM resolution, and the simulation effect is different under different DEM resolutions. Through the SIMWE model, Fernandes found that 91.2% of the break points in the field ridges were located at medium to high water depths, which could better identify the areas where soil was susceptible to gully erosion [15]. Pijl compared the spatial distribution of simulated water depth with the actual spatial distribution of erosion and found that the SIMWE model performed well in identifying soil erosion processes under heavy rainfall conditions [10].

In this study, GIS and SIMWE models were applied for analyzing and predicting soil erosion in the Tongshuang small watershed in the black soil region of Northeast China. Based on the 2.5 cm resolution DEM of unmanned aerial vehicle (UAV) 3D reconstruction, we compare the simulation effect of DEM data input into the SIMWE model with different resolutions, discuss the best resolution of hydrological simulation of sloping cultivated land in the black soil region of Northeast China, and explore the critical water depth of ridge erosion damage. The aim of this study is to provide a theoretical basis and technical

support for the prevention and control of soil erosion on slopes in the black soil region of Northeast China.

2. Materials and Methods

2.1. Study Sites

The study area is located in the Tongshuang small watershed (47°26′31″–47°27′34″ N, 126°17′08″–126°18′40″ E) in Baiquan County, Qiqihar City, Heilongjiang Province (China), with an elevation of 212.6–272.9 m. The study area belongs to a typical middle–high latitude area of water erosion. The main soil types are black soil (Mollisols, USDA, 2011) and meadow soil (Alfisols, USDA, 2011), and the volume contents of sand (0.05–2 mm), silt (0.002–0.05 mm) and clay (<0.002 mm) are 16%, 47.6% and 36.4%, respectively. The bulk density of the soil is 1.07–1.35 g/cm³, and the organic matter content is 3.5% [16]. The soil moisture content is 17.38–26.79%, the soil saturated moisture content is 32.00%–46.89%, and the average groundwater level is less than 2 m [17]. The natural vegetation is mainly red pine, campanula pine and birch, and the main crops are soybean and corn as well as grass crops. The soil and water conservation measures mainly include longitudinal ridge cropping, contour ridge cropping and terracing, etc. The region belongs to a temperate continental monsoon climate, with an average annual temperature of 1.2 °C and an average annual precipitation of 488.2 mm, with more than 70% of the annual precipitation concentrated in July to September [18].

2.2. Digital Elevation Model Acquisition and Processing

In this study, DJI Phantom 4RTK is used for image data collection. The flight relative altitude is 80 m and the course overlap degree and side overlap degree of the photos are 80%. Detailed information of the flight parameter settings is shown in Table 1. Pix4dmapper 4.4.4 is used to process images and generate the point cloud, Digital Orthophoto Map (DOM) and DEM. The resulting DEM errors are shown in Table 2. Based on the 2.5 cm resolution DEM constructed by UAV photogrammetry, DEMs with 0.2 m, 0.5 m, 1 m, 2 m and 5 m resolutions are generated. The 12.5 m resolution DEM is downloaded from the Geospatial Data Cloud (<https://www.gscloud.cn/>, accessed on 1 September 2024).

Table 1. Basic DEM information.

Project	Parameter Value
Area coverage/hm ²	25.26
Flight altitude/m	80
Number of images/n	494
The number of images that have been calibrated/n	494
Ground resolution/(m·pixel ^{−1})	0.02

Table 2. DEM error values.

Project	Azimuth	Parameter Value
Absolute geographic error/m	x	0.018
	y	0.021
	z	0.011
Relative geographic error/m	x	0.05
	y	0.05
	z	0.10

2.3. SIMWE Input

In this study, the rainfall is designed as a 10-year rainstorm in the black soil region, with a rainfall intensity of 50 mm·h^{−1} and a rainfall duration of 60 min (Meteorological data from the “Keshan Experimental Station, Institute of Soil and Water Conservation Science” (125°49′39″E, 48°3′28″N)). Based on the current research findings, the rough-

ness of Manning was determined for different land use and soil and water conservation measures (Table 3) [19–22]. According to the typical black soil texture, the soil separation capacity coefficient is calculated to be $0.0069 \text{ s}\cdot\text{m}^{-1}$ according to the soil separation capacity calculation method of the WEPP model (Equation (1)) [23]. The runoff transport capacity coefficient is estimated to be 0.022 s and the critical shear force is 1.00 Pa in the study area according to the relationship between the soil particles and runoff transport capacity in the study area [24].

Table 3. Input parameters of the SIMWE model.

Measure/Land Use	Manning Roughness	Infiltration Rate ($\text{mm}\cdot\text{h}^{-1}$)
Contour tillage	0.090	36.3
Field ridge	0.067	34.6
Road	0.010	10.0
Break points	0.010	10.0
Wasteland	0.600	30.0

Note: The break points refer to broken ridges or field ridge erosion and destruction point.

$$K_r = 0.0069 + 0.134e^{-20c} \quad (1)$$

where K_r is the soil separation capacity coefficient of $0.0069 \text{ s}\cdot\text{m}^{-1}$; c is the clay content (%).

2.4. Runoff Pathways and Erosion/Sediment Spatial Distribution

The SIMWE model is a spatially distributed model designed for estimating soil erosion caused by single storm events and follows the fundamental theoretical principles of the Water Erosion Prediction Project model (WEPP). However, it does not assume the watershed consists of uniform hillslopes, which allows for fully distributed soil erosion estimation in areas with highly varying topography. It includes the calculation of two modules: the ‘r.sim.water’ and the ‘r.sim.sediment’ [10]. The input parameters include DEMs with different resolutions, their first partial derivatives along the east–west (x) and north–south (y) directions, water depth, soil separation capacity coefficients, runoff transport capacity coefficients, and critical shear forces.

(a) Runoff path calculations: using the Water Flow Motion Simulation Module r.sim.water, which is based on the duality of Saint-Venant equations to describe the movement of bi-dimensional water flows [25],

$$\partial h(r,t)/\partial t = i(r,t) - \nabla q(r,t) \quad (2)$$

where $h(r,t)$ is the water depth (m); t is the time (s); $i(r,t)$ is the net rainfall ($\text{m}\cdot\text{s}^{-1}$); $q(r,t)$ is the flow rate ($\text{m}^3\cdot\text{s}^{-1}$); $r = (x,y)$ represents the plane coordinates of each point; x is the abscissa of each point; and y is the ordinate of each point.

(b) Calculation of erosion/sediment spatial distribution: Using the Soil Erosion Simulation Moduler.sim.sediment. The slope version of the WEPP model is extended to the two-dimensional form, and the sediment transport process of two-dimensional runoff is described through the continuity relationship of sediment quantity [26]:

$$D(r,t) = \frac{\partial[\rho c(r,t)h(r,t)]}{\partial t} + q_s(r,t) \quad (3)$$

where $q_s(r,t)$ is the single wide flux of sediment ($\text{kg}\cdot\text{m}^{-1}\cdot\text{s}^{-1}$); $c(r,t)$ is the sediment concentration ($\text{particle}\cdot\text{m}^{-3}$); ρ is the sediment particle mass ($\text{kg}\cdot\text{particle}^{-1}$); and D is the net erosion/deposition rate ($\text{kg}\cdot\text{m}^{-2}\cdot\text{s}^{-1}$).

2.5. Calculation of Hydrological Index of Connectivity

The index of connectivity (IC) reflects the degree of connectivity between different parts of a watershed. This paper adopts the connectivity index (IC) calculation method improved by Cavalli on the basis of Borselli [27]. The value range of the IC is $(-\infty, +\infty)$. The larger the value, the better the hydrological connectivity. The calculation method is as follows [26]:

$$IC_k = \lg\left(\frac{D_{up,k}}{D_{dn,k}}\right) = \lg\left(\frac{\overline{W_k} \cdot \overline{S_k} \cdot \sqrt{A_k}}{\sum_i \frac{d_i}{\overline{W_i} \cdot \overline{S_i}}}\right) \quad (4)$$

where D_{up} is the upslope component of connectivity, reflecting the potential of the upslope catchment to contribute water flow; D_{dn} is the downhill component of connectivity and represents the length of the flow path that water must travel to reach the nearest target or catchment area. W_k is the weight factor (dimensionless) of the roughness of the underlying surface of the upslope catchment. S_k is the average slope of the upslope catchment (m/m); A_k is the area of uphill catchment (m^2); d_i is the distance (m) between the i grid and the pixel at the catchment point along the water flow path; and W_i and S_i are the weight factor and slope of the i grid, respectively.

The roughness of the surface will affect the flow and sediment transport, and the weight factor W reflects the influence of different land use and surface conditions on the roughness of the surface and has an impact on the runoff and sediment transport process [27,28]. Researchers have improved the weight factors in different ways, such as by using the vegetation cover and management factors of the general soil loss equation, roughness index, normalized difference vegetation index (NDVI), Manning roughness ratio, etc., as weight factors [28–30]. In this study, the relative smoothness index calculated by the Manning roughness coefficient is used as the weight coefficient, and the calculation method is as follows [31]:

$$W_{RS} = n_{\min}/n \quad (5)$$

where W_{RS} is the dimensionless relative smoothness index, with the value ranging from 0 to 1; n_{\min} is the minimum value of local Manning roughness. n is the Manning roughness coefficient of different land uses or measures.

2.6. Surface Feature Point Recognition Method

Based on the 2.5 cm resolution DEM generated by UAVs, the surface feature points (fields, field ridges, break points, roads, forest lands, etc.) in the study area are identified through artificial visual interpretation of DOM images (Figure 1). Hue, texture, shape, position and structural features in the DOM are interpreted with field-observed erosion, and feature point information is extracted by ArcGIS.



Figure 1. Overview of study area.

2.7. Relative Elevation Difference Calculation

Based on the 2.5 cm resolution DEM obtained by UAVs, the average elevation line is drawn by ArcGIS. Based on this elevation line, the average elevation plane is made and superimposed with DEMs of different resolutions to obtain the relative elevation difference in DEM points of different resolutions $d_i = D_i - D_i'$ (D_i is the elevation of each point of the average elevation plane. D_i' is the elevation of DEM points of different resolutions).

2.8. Statistical Analysis

Statistical analyses were accomplished in IBM SPSS Statistics 22.0 (IBM Corp., Armonk, NY, USA). An analysis of variance (ANOVA) was conducted to determine the significant differences between the average water depth and the average water depth per unit length between the area with and without the damage points. The least significant difference (LSD) method was applied at the 95% confidence level for comparisons. A Pearson correlation matrix was performed to illustrate the correlations of erosion, the relative elevation difference, and the runoff water depth.

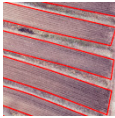

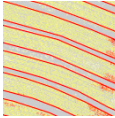


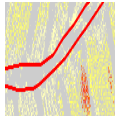


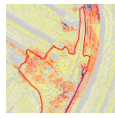
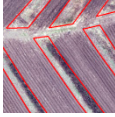

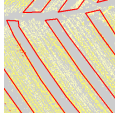


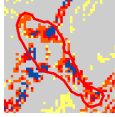
3. Results and Analysis

3.1. Effect of DEM Resolution on Spatial Distribution of Erosion Features

3.1.1. Interpretation Characteristics of Typical Ground Objects and Their Erosion Characteristics

Image interpretation marks are the image features that directly reflect and distinguish ground object information on remote sensing images. Through comparative analysis of image data and field topography, the interpretation markers of remote sensing images are established. The interpretive signs of the objects in the study area are shown in Table 4.

Table 4. Interpreting markers and erosion signatures.

Number	Surface Feature Points	Image Feature	Remote Sensing Image	Live Photo	Erosion Legend	Area/m ²
1	Cultivated land	Brown, shape is a long block				95,212.10
2	Field road	Gray-white, shape is long and narrow				1021.87
3	Wasteland	Gray-green, flaky shape				1321.82
4	Field ridge	Gray-green, long block shape				37,045.52
5	Break point	Brown, irregular shape				38.27

According to the established interpretation markers, based on the 2.5 cm resolution DEM data generated by UAVs, computer-aided classification combined with DOM remote sensing images was used for manual visual interpretation and recognition, and the surface

feature points in the study area were identified in the order from known to unknown, first overall, then local, first macro and then micro. Based on the analysis and interpretation of the color, shape and other features of the target ground objects in the remote sensing image, the types of objects in various places are inferred (Figure 2).

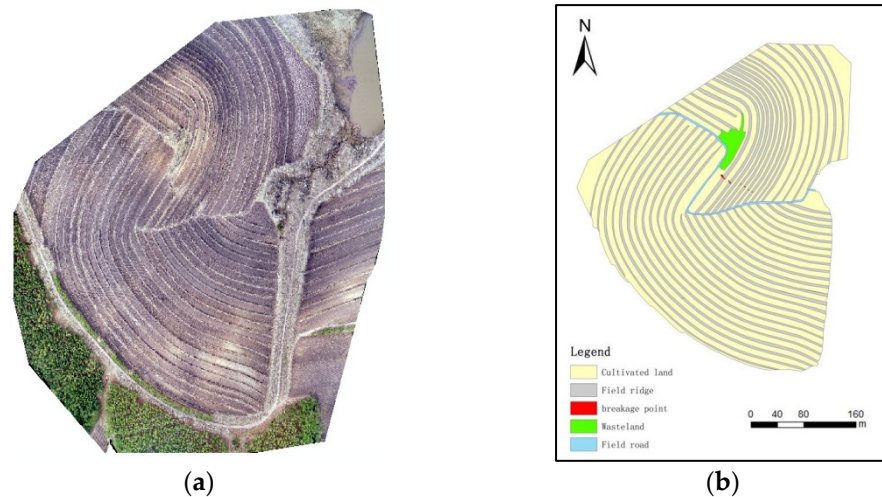


Figure 2. (a) Digital Orthophoto Map of the study area. (b) Map of land surface feature point identification.

The visual interpretation method was used to obtain the area of object types in different DEM resolutions, and the obtained area was divided by the area of object types in the reference map of surface feature points to calculate the ratio of corresponding object areas, which was used to evaluate the accuracy of interpretation (Table 5). The results show that the accuracy of ground object interpretation varies with DEM resolution. The interpretation area ratio of cultivated land and wasteland decreases with the decrease in DEM resolution, while the interpretation area ratio of cultivated land decreases first and then increases. With the decrease in DEM resolution, the interpretive area ratio of the field road and field ridge gradually decreases, while the interpretive area ratio of the field ridge first increases and then decreases. The break points are represented in the form of points, and the interpretive area ratio increases first and then decreases with the decrease in DEM resolution. When the DEM resolution is 0.2 m, the ratio of interpretation area of the field road, wasteland, break point, field ridge and cultivated land is 92.55%, 93.87%, 109.47%, 98.02% and 100.93%, respectively, with the maximum difference within 10%, which can be basically considered consistent with the reference map area of local objects.

Table 5. Evaluation table of interpretation accuracy of each land type (%).

Land Type	DEM Resolution			
	0.2 m	0.5 m	1 m	2 m
Field road	92.55	84.77	72.87	68.38
Wasteland	93.87	86.85	82.73	77.88
break point	109.47	136.81	171.21	62.59
Field ridge	98.02	129.11	120.21	115.80
Cultivated land	100.93	89.00	92.64	94.52

The feature points of different ground surface vary obviously with DEM resolution, which is mainly related to their size. There is a certain “response relationship” between the resolution and interpretation of surface features, that is, the way in which the surface features in images respond to changes in resolution [32]. The break points are represented in the form of dots, which can be more accurately captured and interpreted at high resolution. The width of the break points in the study area ranges from 0.3 m to 1.5 m. When the

DEM resolution is 0.5 m or 1 m, some areas will be identified in a grid with cultivated land and field crests, resulting in an increase in the ratio of the interpretation area of the break points. However, when the DEM resolution is greater than 2 m, the break point is difficult to capture and interpret, resulting in an obvious reduction in the interpretive area ratio. Surface features such as cultivated land and wasteland can still be identified when the resolution is reduced, so the ratio of interpreted area of the wasteland will decrease with the decrease in DEM resolution. However, low-resolution images cannot accurately reflect the subtle changes inside the features. For linear surface features such as field roads and ridges, the interpretation accuracy is mainly affected by their widths. The width of field roads in the study area is about 2 m. When the DEM resolution is 0.2 m–2 m, with the decrease in DEM resolution, some field roads are misinterpreted as other surrounding surface feature points (cultivated land, ridges, etc.). As a result, the ratio of field interpretation area decreases with the decrease in resolution. When the DEM resolution is 0.5 m, part of the cultivated land is misinterpreted as a field ridge, resulting in a large increase in the ratio of interpreted area. Then, with the decrease in the DEM resolution, part of the field ridge is misinterpreted as cultivated land, etc., so that the interpreted area gradually decreases. In this study area, the visual interpretation effect is better when the DEM resolution is 0.2 m–1 m, and the interpretation effect is best when the DEM resolution is 0.2 m.

3.1.2. Erosion Distribution Characteristics

Based on DEM data, the distributed hydrological model can simulate the changes in water and sediment in the area and reflect the spatial distribution characteristics of erosion on the land surface. The SIMWE model is sensitive to the change in DEM resolution, based on the resolution of 0.2 m, 0.5 m, 1 m, 2 m, 5 m and 12.5 m DEM modeling of the erosion deposition distribution in the study area (Figure 3a–f). The spatial distribution of erosion deposition varies obviously under different DEM resolutions. In general, the part with severe erosion intensity is generally located in the low-lying position with large relative elevation difference. With the decline in DEM accuracy, the intensity of severe erosion gradually becomes less obvious. When the DEM resolution is 2 m, it is basically impossible to judge the location of erosion. However, for DEM resolutions of 5 m and 12.5 m, the spatial distribution map of erosion and deposition presents rasterization, which fails to show the morphological characteristics of object types in different places, and there is a certain deviation to the erosion simulation results.

Different typical soil and water conservation measures have different performances in reducing soil erosion degree, and the DEM resolution will affect the information expression of each measure. Under different DEM resolutions, the field roads and ridges did not show obvious erosion phenomenon; most of the cultivated land showed slight erosion, some had a mild to extremely strong and above erosion degree, the wasteland showed mild to moderate erosion, and the erosion at the break point was strong and above. Under the 0.2 m resolution DEM, the parts of cultivated land with strong erosion intensity and above are generally displayed along the low terrain of each section of cultivated land, the erosion intensity is strong and above at the break point, and the erosion intensity around the break point is mainly strong, followed by extremely strong and above. The spatial distribution of erosion deposition can show different degrees of erosion intensity from slight to extremely strong and above. When the DEM resolution is 0.5 m, there is almost no extremely strong erosion intensity on the cultivated land, the width of moderate or strong erosion is greatly reduced, the break point is dominated by strong erosion, there is a small amount of extremely strong erosion or above, the cultivated land around the break point is dominated by moderate or strong erosion, and the overall area of mild erosion intensity in the erosion deposition spatial distribution map is remarkably reduced. Under the 1 m resolution DEM, the width of moderate or strong erosion of cultivated land decreases, the break point is mainly moderate or strong erosion, and the cultivated land around the break point is mainly mild or moderate erosion, with a small amount of strong erosion; the spatial distribution map of erosion and deposition basically has no strong erosion. When the DEM

resolution is 2 m, there is a small amount of mild erosion on cultivated land, followed by moderate erosion, and the erosion width is small; there is basically no strong erosion in the erosion deposition spatial distribution map. Under the 5 m resolution DEM, the spatial distribution map of erosion and deposition is dominated by slight erosion, with very little mild erosion and moderate erosion. When the DEM resolution is 12.5 m, there is no mild erosion or moderate erosion in the spatial distribution map of erosion deposition, and only very strong erosion or above exists at the edge of the map.

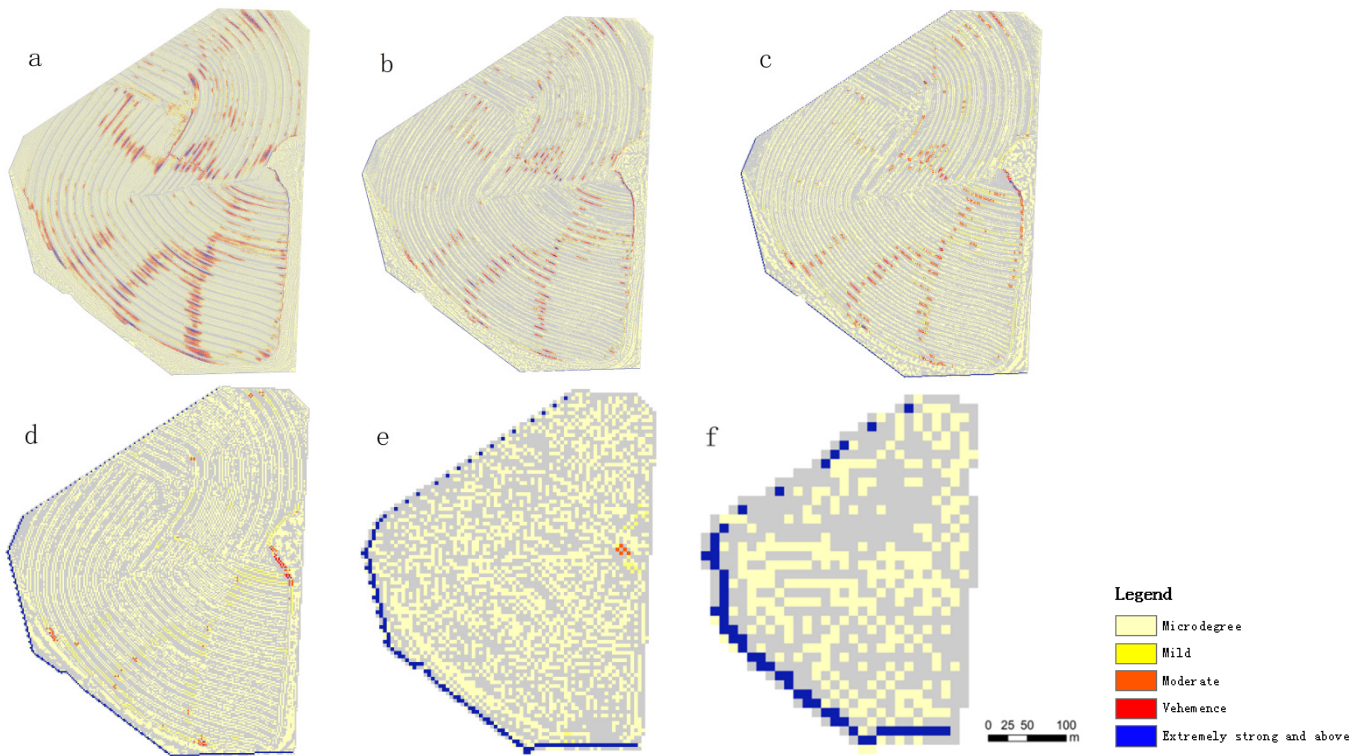


Figure 3. Spatial distribution characteristics of erosion sedimentation at different DEM resolutions. (a) 0.2 m resolution, (b) 0.5 m resolution, (c) 1 m resolution, (d) 2 m resolution, (e) 5 m resolution, (f) 12.5 m resolution. Microdegree: $<6.34 \times 10^{-9} \text{ kg}/(\text{m}^2 \cdot \text{s})$. Mild: $6.34 \times 10^{-9} - 7.93 \times 10^{-8} \text{ kg}/(\text{m}^2 \cdot \text{s})$. Moderate: $7.93 \times 10^{-8} - 1.59 \times 10^{-7} \text{ kg}/(\text{m}^2 \cdot \text{s})$. Vehemence: $1.59 \times 10^{-7} - 2.54 \times 10^{-7} \text{ kg}/(\text{m}^2 \cdot \text{s})$. Extremely strong and above: $>2.54 \times 10^{-7} \text{ kg}/(\text{m}^2 \cdot \text{s})$.

From the perspective of the area of soil erosion intensity at all levels (Table 6), when the DEM resolution decreases from 0.2 m to 2 m, with the decrease in DEM resolution, the area of slight erosion generally presents an upward trend, the area of mild erosion and extremely strong erosion or above presents an increasing trend and then a decreasing trend, and the area of moderate erosion and strong erosion generally presents a decreasing trend. Harini and Vaze et al. found that for small-scale surface features with obvious surface morphological changes (such as ridges, roads, etc.), the DEM resolution is higher than the size of the surface features and the calculation results of the model are more accurate [33,34]. When the DEM resolution decreases from 0.2 m to 2 m, the proportion of the micro-erosion area is 75.71%, 89.74%, 88.18% and 90.63%, respectively, which increases conspicuously when the DEM resolution is 0.5 m. Because micro-erosion is mainly manifested in cultivated land, some cultivated land is misinterpreted as field ridge when the DEM resolution is 0.5 m. There is no obvious erosion phenomenon, so the overall erosion area decreases, and the proportion of the slight erosion area increases greatly. However, when the DEM resolution is 1 m and 2 m, the field and sill area decreases, while the non-obvious erosion area decreases, the overall erosion area increases, and the proportion of slight erosion area increases. The proportion of the light erosion area is 13.33%, 6.11%, 7.87% and 6.43%, respectively. As light erosion is mainly manifested in the side of cultivated land along

the low terrain, when the DEM resolution is 0.5 m, the cultivated land area is reduced, the light erosion area is greatly reduced, and the proportion of the light erosion area is conspicuously reduced. With the increase in cultivated land area, the proportion of slightly eroded area increases. When the DEM resolution is 2 m, the area of slightly eroded land increases and the area of mildly eroded area decreases, while the proportion of mildly eroded area decreases. The proportion of moderate erosion area and strong erosion area decreases with the decrease in resolution. The main reason is that the DEM resolution decreases, the expression of topographic details is lost more, and surface features such as break points cannot be fully expressed, so the areas of moderate erosion and strong erosion decrease, and the area proportion of both decreases. The proportion of extremely intense and above erosion area is 1.73%, 0.81%, 1.22% and 2.29%, respectively, and the extremely intense and above erosion area is mainly manifested in the break point and the cultivated land around the break point. When the DEM resolution is 0.5 m, due to the reduction in the cultivated land area, the extremely intense and above erosion area on the cultivated land decreases, and the proportion of the erosion area decreases conspicuously. When the DEM resolution is 1 m and 2 m, the area of extremely severe and above erosion increases, and the proportion of erosion area increases. When DEM resolution is 5 m and 12.5 m, the area of slight erosion is greatly reduced, the area of mild erosion, moderate erosion and strong erosion is basically 0, and the area of extremely severe erosion and above is slightly increased. When the DEM resolution is greater than 5 m, the erosion deposition distribution map is basically controlled by topography, and the surface micro-topography such as break points cannot be expressed. As a result, parameters such as slope, slope length, confluence area and LS value change, and there is a certain deviation in the calculation of soil erosion intensity [35–37].

Table 6. Percentage of area with different resolutions of soil erosion intensity (%).

Resolution	Erosion Intensity	Microdegree	Mild	Moderate	Vehemence	Extremely Strong and Above
0.2 m		75.69	13.33	6.51	2.75	1.73
0.5 m		89.75	6.11	2.53	0.81	0.81
1 m		88.14	7.87	2.44	0.33	1.22
2 m		90.63	6.43	0.54	0.11	2.29
5 m		93.66	0.73	0.24	0.00	5.37
12.5 m		84.82	0.00	0.00	0.00	15.18

Figure 4 shows the spatial distribution of the correlation coefficient between erosion loss and relative height difference in the study area with a DEM resolution of 0.2 m, showing a positive correlation as a whole. When the relative height difference is 0.2–0.5 m, the correlation coefficient between the erosion and relative height difference is between 0.43 and 0.92, and the spatial average correlation coefficient is 0.74. When the DEM resolution is 0.2 m, the correlation between erosion and relative height difference can be accurately reflected.

With the development of computer technology and measurement technology, the high-resolution DEM has become more common, making hydrological model simulation results more accurate. In terms of the small-scale slope erosion simulation effect, when the DEM resolution is about 1 m, it can characterize the spatio-temporal distribution characteristics of erosion and deposition at large, while when the DEM resolution is higher, it can better describe small-scale ground objects with rich details, achieve better interpretation accuracy and make the simulation results more accurate. Therefore, for different research scales, the resolution selection of the DEM has different requirements, and the resolution should be selected according to the characteristics of the research area, that is, the size of the minimum key ground objects to be identified [28]. For the whole research area, when the DEM resolution is 0.2 m–1 m, the visual interpretation can better interpret the surface feature points in the area, but when the DEM resolution is greater than 0.2 m, there is

a certain loss in the expression of surface feature information such as cultivated land, resulting in deviations in the calculation of soil erosion intensity by the SIMWE model. In order to better simulate the erosion deposition distribution in the region, the optimal DEM resolution is 0.2 m.

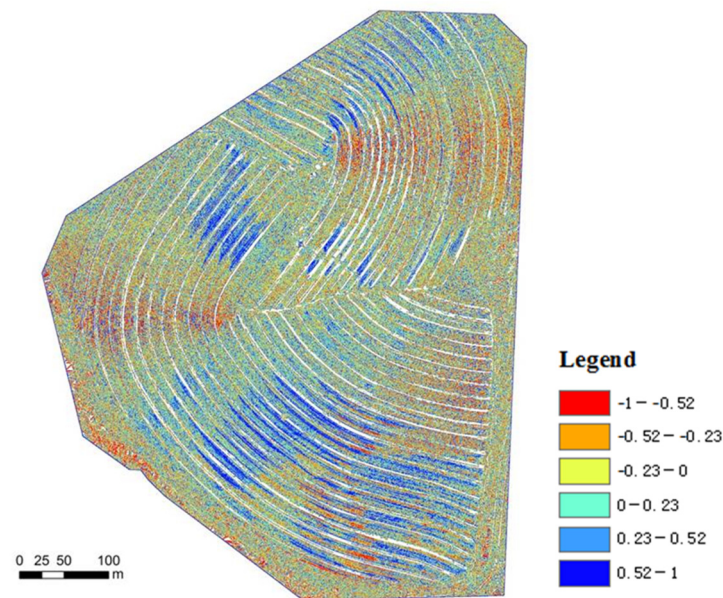


Figure 4. Spatial distribution of correlation coefficient between erosion amount and relative height difference.

3.2. Critical Depth Calculation

Surface runoff is the key driving force of soil erosion on slopes. Soil erosion occurs when the erosion force of surface runoff exceeds the critical shear strength of soil. The study of runoff paths can reveal the process of runoff and sediment transport, effectively manage runoff and provide references for slope erosion prevention and control [38]. The spatial distribution of water depth in the study area was obtained based on DEM with 0.2 m resolution (Figure 5). The runoff flows along the ridge, and under the influence of the surface microtopography, the runoff will gather in the low-lying position of the ridge, forming shallow gully catchment area, and the soil erosion will be intensified. The places where water flows together are often places where erosion intensity is intense. The Pearson correlation analysis showed that soil erosion was significantly correlated with runoff depth ($R = 0.33$, $p < 0.05$). Wang L and Shen H O found through an indoor soil trough erosion experiment that ridge breaking would occur when the water depth reached about 0.3 m, that is, when the water exceeded the holding capacity of the ridge, the ridge was destroyed, the ability of the ridge to hold runoff was weakened and the soil erosion amount increased [11,12].

After heavy rainfall, surface runoff flows along the terrace with the terrain, converges at the field ridge and concentrates in the local depression of the field ridge, resulting in soil erosion. After several heavy rainfalls, the field ridge is damaged. Through visual interpretation and field-observed erosion, six break points were found in region I of the study area (Figure 6), while no break points were found in region II with the largest water depth. In order to explore the critical water depth value of ridge erosion damage, this paper, based on the progressive triangulation filter algorithm, manually classified the point cloud and reconstructed the undamaged terrain. The spatial distribution of the water depth in region I after reconstruction is shown in Figure 7.

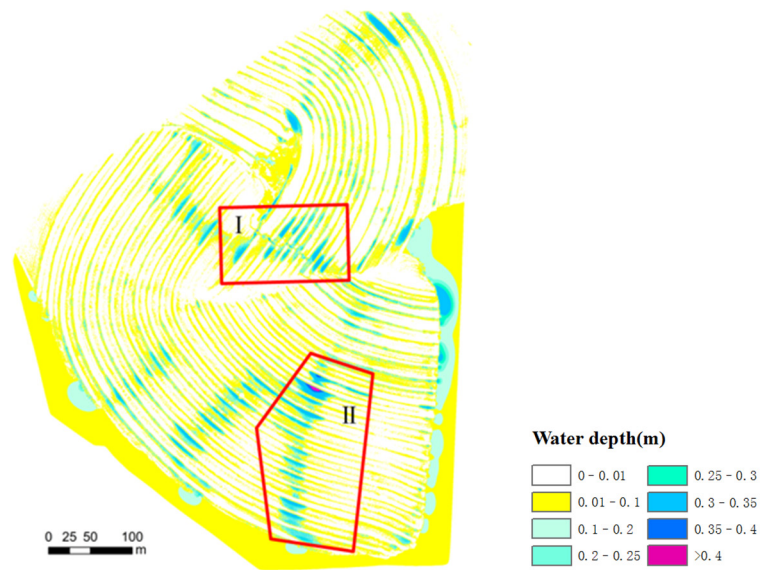


Figure 5. Spatial distribution map of water depth with 0.2 m DEM resolution.

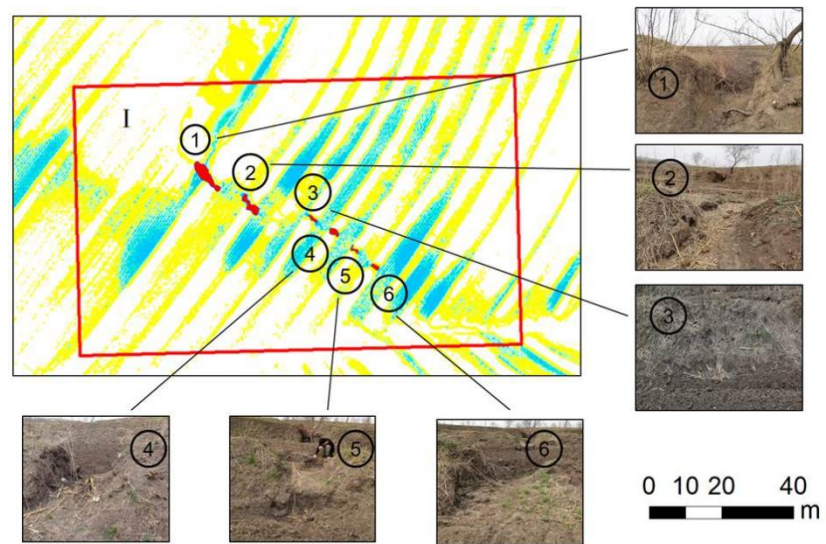


Figure 6. Site investigation map.

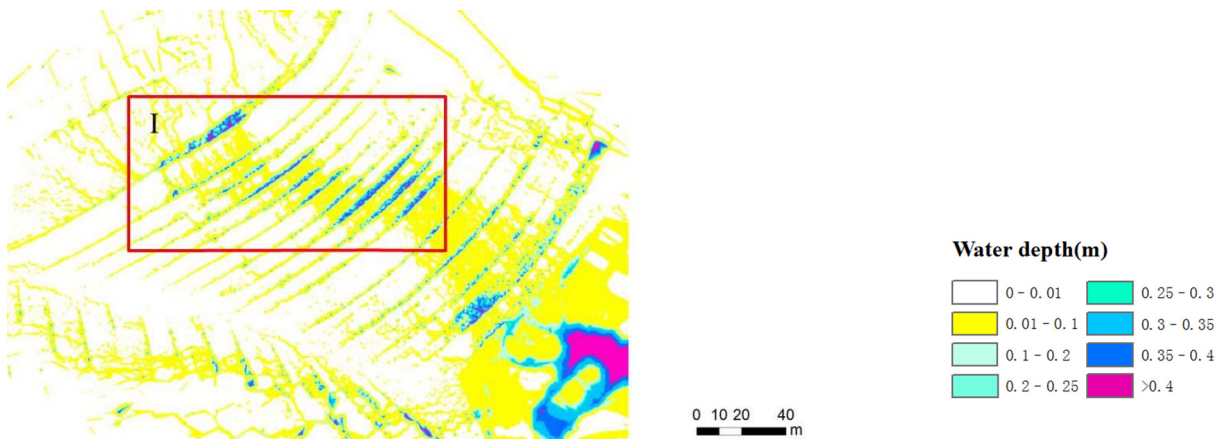


Figure 7. Spatial distribution map of water depth of undamaged terrain.

In order to reduce the influence of local topographic depression on water depth calculation factors, a $1\text{ m} \times 1\text{ m}$ grid was made for the maximum water depth of each ridge of the reconstructed terrain and the same position of the original terrain, and the water depth in the grid was calculated on average. The results are shown in Table 7. According to the actual field survey, erosion damage has occurred in fields and ridges, and the water depth calculated by the model is the potential water depth. The original terrain water depth has reached the critical water depth, and the critical water depth ranges from 0.335 m to 0.359 m.

Table 7. Ridge depth calculation table of reconstructed terrain and original terrain.

Confluence Length (m)	Gradient	Reconstructed Terrain Water Depth (m)	Pristine Terrain Water Depth (m)
80	0.0218	0.338	0.320
80	0.0181	0.335	0.304
81	0.0167	0.359	0.324
82	0.0152	0.341	0.317
83	0.0179	0.342	0.317
83	0.0162	0.359	0.323

In order to reduce the influence of local topographic depression on water depth calculation factors, a $1\text{ m} \times 1\text{ m}$ grid was made for the maximum water depth of each ridge in region I and region II, and the water depth in the grid was calculated on average. The results are shown in Table 8. The average water depth in the two regions is near the critical water depth range, and there is no significant difference between the two groups of data. In this study, the ratio of average water depth to confluence length, which is the average water depth per unit length, indicates the critical range of ridge damage. The average water depth per unit length in region I is less than 0.0040, and the average water depth per unit length in region II is more than 0.0045. The difference between the two groups of data is analyzed, $p < 0.05$, and there is a significant difference. When the water depth per unit length is between 0.0040 and 0.0045, it is in the critical range of ridge damage.

Table 8. Calculation table of average water depth of ridges.

	Confluence Length (m)	Average Water Depth (m)	Average Water Depth per Unit Length (m/m)
region I	80	0.320	0.0040
	80	0.304	0.0038
	81	0.324	0.0040
	82	0.317	0.0039
	83	0.317	0.0038
	83	0.323	0.0039
region II	65	0.332	0.0051
	66	0.316	0.0048
	66	0.312	0.0047
	68	0.315	0.0046
	68	0.306	0.0045
	70	0.318	0.0045
	70	0.328	0.0047
70	0.328	0.0047	

According to the spatial distribution of water depth simulated by the SIMWE model, when the water depth is 0.335–0.359 m, the potential erosion risk can be preliminarily judged. When the average water depth per unit length ranges from 0.0040 to 0.0045, the ridge is in the critical range for the occurrence of ridges; when the average water depth per unit length is less than the critical range, ridge erosion damage occurs. When the ridge is larger than the critical range, no damage has occurred, but there is a potential erosion risk.

The above results can provide some theoretical reference for predicting the erosion damage of ridges.

3.3. Prediction of Erosion by Hydrological Connectivity

Hydrological connectivity can reflect the smoothness or hindrance degree of watershed units. Changes in hydrological connectivity will have a remarkable impact on erosion and sedimentation processes and are closely related to soil erosion intensity [39]. When local erosion damage occurs, the degree of connectivity will change dramatically, and whether erosion damage occurs can be judged by the change in IC index. Figure 8 shows the IC distribution map of hydrological connectivity index in the study area generated based on a 0.2 m resolution DEM. In region I, the mean IC of cultivated land was -2.18 , while the mean IC of cultivated land was -4.93 , which increased by 126.1% on average, and the connectivity increased conspicuously. The average IC value of cultivated land in region II was -2.71 , and there were a few mutation points, which increased by 24.1% compared with the average IC value of cultivated land in region I, and the change area was not obvious.

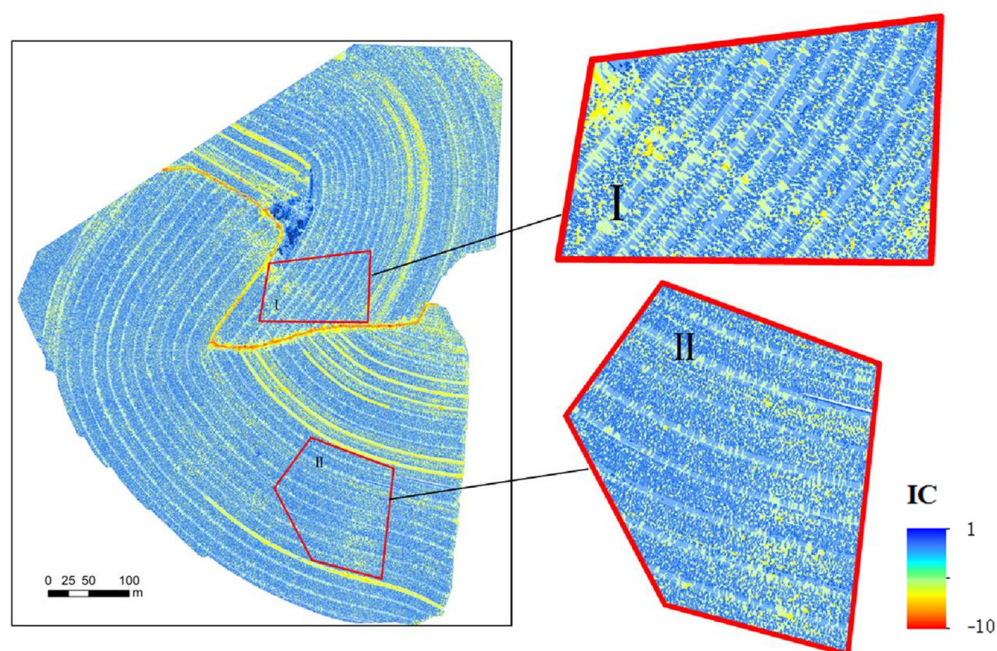


Figure 8. A 0.2 m resolution DEM surface hydrological connectivity index distribution map.

Figure 9 shows the frequency distribution of ICs for region I and region II. In region I, the frequency of IC -4 is the largest, which is 40.8%, and a few IC values are about -7 . The frequency of region II with an IC of -3 is the highest (46.3%), and there are a few ICs that reach about -6 . The area of the grid frequency curve with an IC value -7 ~ -4 and an X-axis is obviously smaller than that of region I, and the hydrological connectivity is small. It can be seen that no erosion damage has occurred in the ridge in region II, while ridge damage has occurred in region I. When the IC value changes dramatically with the surrounding IC value, it can provide a reference for predicting the erosion damage.

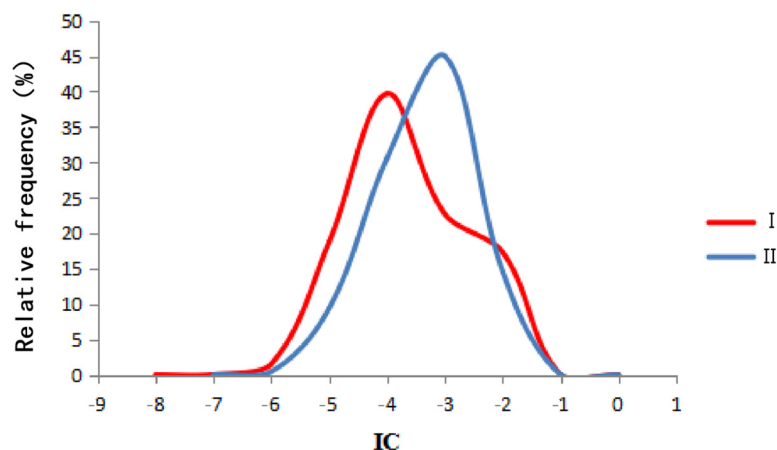


Figure 9. Frequency distribution of connectivity index (IC) in regions I and II.

4. Discussion

4.1. Limitations of Erosion Distribution Research

The temporal and spatial distribution of erosion and sedimentation is a complex process. Although there are methods such as nuclide tracing, REE tracing and control condition experiments, the true value of the spatial distribution under historical conditions cannot be obtained. In this study, we focused primarily on the effects of erosion. Due to the insufficient consideration of the relationship between water and sediment transport, the attention to sedimentation is reduced. This will be further strengthened in future research.

4.2. The Effectiveness of SIMWE Model in Predicting Ridge Damage

In this study, the water depth range simulated based on the SIMWE model was mainly distributed within <0.1 m under the condition of 50 mm/h rain intensity, and the runoff flow along the ridge led to runoff collection in low-lying areas, with a water depth range of more than 0.3 m. The places where runoff converged were often the locations of severe erosion distribution (Figures 3 and 5). The result shows that when the water depth range is 0.335–0.359 m, it can be preliminarily judged that there is a potential erosion risk in the area, that is, there is a possibility of ridge damage (Figure 6, Table 7), which is consistent with the phenomenon that Wang L and Shen H O found in that the ridge is very prone to damage when the water depth is about 0.3 m, based on an indoor soil trough scouring experiment; this shows that the spatial distribution characteristics of water depth simulated by the SIMWE model and the critical water depth range of ridge damage are relatively reasonable. However, in this study, the critical water depth could not effectively determine the damage characteristics of all ridges, and there was a phenomenon that ridge damage did not occur beyond the critical water depth (Figure 5, region II.). Based on this, this study further proposes the concept of average water depth per unit length to determine the runoff characteristics of critical failure of ridges, that is, the ratio of average water depth to confluence length within the study area. The result shows that the average water depth per unit length of ridge damage is between 0.0040 and 0.0045 m/m (Table 8). Under this critical range, all areas found to be damaged by erosion can be correctly marked, and the areas without erosion damage are not marked. The result shows that the average water depth per unit length is more effective than water depth in judging the damage characteristics of ridges. In addition, the IC value increased abruptly at the location of erosion (Figure 8), and the spatial distribution of the abrupt change in the hydrological connectivity index is consistent with the location of ridge damage marked by the average water depth per unit length, which shows that the average water depth per unit length is a reference for the erosion prediction of the critical damage of the ridge.

4.3. Planning Recommendations for Slope Engineering Measures

The protection benefits of terraces on slope soil erosion are reflected in the fact that they can weaken the source–sink relationship in the basin, reduce the hydrological connectivity, change the original flow path of the slope and ultimately affect the slope production and confluence process and the spatial distribution characteristics of sediment erosion, transport and sedimentation on the slope. On the whole, the influence of terraces is mainly reflected in the formation of runoff paths, and some previous studies have shown that the obvious fracture failure of the ridge sections of terraced fields is mainly related to the large collection of runoff. This is also evidenced by the experimental results of this study, where the water depth and average water depth per unit length of ridge damage are a lot larger than those at other locations on the slope (Figure 6). The hydrological connectivity index also increased conspicuously at these locations (Figure 8), and soil erosion increased at the point of damage (Figure 4), which is consistent with the results of previous studies. The development of ridge break points will lead to a large accumulation of surface water and an obvious increase in hydrological connectivity, which will lead to a vicious cycle of destruction–confluence–destruction, resulting in serious erosion of terraces. Therefore, in view of the topographic characteristics of the black soil area in Northeast China, which is dominated by long and gentle slopes and is prone to form a large number of slope confluences, the construction of terraces should comprehensively consider the rainfall characteristics and the water depth distribution characteristics caused by the slope confluence area. Based on the results of this study, when water depth reaches the range of 0.335 m–0.359 m on the slope, and the average water depth per unit length is in the range of 0.0040–0.0045 m/m, appropriate retaining and drainage measures should be considered to control the risk of ridge damage, reduce soil erosion and maintain the terraces.

Due to the short observation time, it was not possible to obtain topographic data of the terraces without erosion and damage, and when calculating the critical water depth, the original topography could only be roughly restored by filtering and manually screening point clouds. In order to better maintain the terraces and the follow-up research needs, it is recommended to start regular long-term monitoring when the terraces are laid out to form a long series of monitoring data through model simulation and analysis, design and plan schemes and interception and drainage measures in the potential erosion risk area, where runoff collects, to reduce the possibility of terrace damage.

5. Conclusions

In this paper, we take the Tongshuang small watershed as the research object to explore the critical water depth range of erosion and damage in the terraced ridges of sloping cultivated land in the black soil region of Northeast China. Based on the SIMWE model, the study analyzes the best DEM resolution that can reflect the erosion sedimentation characteristics and give the erosion spatial distribution map of the watershed and the critical water depth of ridge failure. The main findings are as follows:

(1) In terms of the simulation effect of small-scale slope erosion, when the DEM resolution is about 1 m, the difference in interpretation accuracy of other ground objects is 7.36–27.13%, except for break points, which can accurately characterize the temporal and spatial distribution characteristics of erosion and sedimentation. When the DEM resolution is increased to 0.2 m, it can better describe small-scale detailed ground objects, achieve better interpretation accuracy and make the simulation results more accurate. Compared with the 2 m resolution DEM, the interpretation accuracy of field roads, wasteland, damaged points, fields and cultivated land at the 0.2 m resolution is improved by 4.55–27.94%, which is the best resolution in the study area.

(2) According to the spatial distribution of water depth simulated by the SIMWE model, when the water depth is 0.335–0.359 m, the potential erosion risk can be preliminarily judged. When the average water depth per unit length ranges from 0.0040 to 0.0045, the ridge is in the critical range for the occurrence of ridges; when the average water depth per unit length is less than the critical range, the ridge is in the critical range. When the ridge

erosion damage is greater than the critical range, ridge damage has not occurred but there is potential erosion risk, which can provide a certain theoretical reference for predicting ridge erosion damage.

(3) Hydrological connectivity can reflect the smoothness or hindrance degree of basin units. When local erosion damage occurs, the degree of connectivity will change abruptly, and the remarkable change in the IC index can provide a reference for predicting erosion damage.

Author Contributions: Conceptualization, M.L.; methodology, Z.C.; software, M.L.; validation, B.W.; formal analysis, M.L.; investigation, M.L. and S.L.; resources, B.W.; data curation, M.L.; writing—original draft preparation, M.L.; writing—review and editing, B.W. and W.W.; visualization, M.L.; supervision, B.W. and W.W.; project administration, B.W.; funding acquisition, B.W. All authors have read and agreed to the published version of the manuscript.

Funding: This study was supported by the National Natural Science Foundation of China (NSFC). Dynamic process and quantification of hybrid soil erosion in black soil region induced by freeze-thaw and water" (Founding number: 41977060) and the National Key R&D Program of China (Founding number: 2016YFE0202900).

Data Availability Statement: The data that support the findings of this study are available from the corresponding author upon reasonable request.

Conflicts of Interest: The authors declare that they have no known competing financial interests or personal relationships that could have appeared to influence the work reported in this paper.

References

- Zheng, F.L.; Wang, Z.L.; Yang, Q.K. Development strategy on soil erosion science in China. *Res. Soil Water Conserv.* **2004**, *4*, 1–10. (In Chinese)
- Liu, Z. Soil and water conservation survey in China and its application. *Sci. Soil Water Conserv.* **2013**, *11*, 1–5. (In Chinese)
- Wang, C.F.; Zhang, S.H.; Wang, B.; Wang, Y.; Wang, Y.; Hu, B.; Wang, K. Study on critical hydraulic characteristic of soil detachment and soil shear strength under different antecedent soil moisture contents. *J. Soil Water Conserv.* **2017**, *31*, 91–96+102. (In Chinese)
- He, Y.X.; Zhang, F.B.; Yang, M.Y. Effects of soil erosion on organic carbon fractions in black soils in sloping farmland of Northeast China by using¹³⁷Cs tracer measurements. *Trans. Chin. Soc. Agric. Eng. (Trans. CSAE)* **2021**, *37*, 60–68. (In Chinese)
- Zheng, F.L. *Characteristics and Prevention of Composite Soil Erosion in the Black Soil Area of Northeast China*; Science Press: Beijing, China, 2020. (In Chinese)
- Li, R.F.; Xie, Y.; Xin, Y.; Yang, J.Y.; Liu, G.; Lin, H.H. Soil infiltration characteristics and simulation of different eroded degrees in the black soil region of Northeast China. *Sci. Soil Water Conserv.* **2004**, *22*, 17–24. (In Chinese)
- Wen, Y.H.; Wang, L.X.; Liu, T.J. Process of runoff and sediment generation on different slopes with ridged cropping in the black soil area of Northeast China. *Res. Soil Water Conserv.* **2022**, *29*, 8–13+20. (In Chinese)
- Tian, Y.; Li, F.M.; Liu, P.H. Economic analysis of rainwater harvesting and irrigation methods, with an example from China. *Agric. Water Manag.* **2003**, *60*, 217–226.
- Tarolli, P.; Sofia, G.; Calligaro, S.; Prosdocimi, M.; Preti, F.; Fontana, G.D. Vineyards in Terraced Landscapes: New Opportunities from Lidar Data. *Land Degrad. Dev.* **2015**, *26*, 92–102.
- Pijl, A.; Reuter, E.L.; Quarella, E.; Vogel, T.A.; Tarolli, P. GIS-based soil erosion modelling under various steep-slope vineyard practices. *Catena* **2020**, *193*, 104604.
- Wang, L.; He, C.; Zheng, F.L.; Bian, F.; Qin, C.; Xu, X.M. Soil-bin experiment on effects of contour ridge tillage for controlling hillslope soil erosion in black soil region. *Trans. Chin. Soc. Agric. Eng. (Trans. CSAE)* **2018**, *34*, 141–148. (In Chinese)
- Shen, H.O.; Wen, L.L.; Wu, J.L.; Wang, Y. Review on the effects of ridge pattern and ridge-furrow intervals on soil erosion of sloping farmland in the black soil region. *Trans. Chin. Soc. Agric. Eng. (Trans. CSAE)* **2022**, *38*, 52–62. (In Chinese)
- Cavazzi, S.; Corstanje, R.; Mayr, T.; Hannam, J.; Fealy, R. Are fine resolution digital elevation models always the best choice in digital soil mapping? *Geoderma* **2013**, *195–196*, 111–121. [[CrossRef](#)]
- Shi, B.; Ren, Z.; Meng, P.F.; Jia, T.F. Impact of DEM Resolution on Hydrological Simulation Accuracy of VIC Model. *Pearl River* **2020**, *41*, 61–66. (In Chinese)
- Fernandes, J.; Bateira, C.; Soares, L.; Faria, A.; Oliveira, A.; Hermenegildo, C.; Moura, R.; Gonçalves, J. SIMWE model application on susceptibility analysis to bank gully erosion in Alto Douro Wine Region agricultural terraces. *Catena* **2017**, *153*, 15339–15349. [[CrossRef](#)]
- Luo, C.; Zhang, W.Q.; Zhang, X.L.; Liu, H.J. Mapping soil organic matter content using Sentinel-2 synthetic images at different time intervals in Northeast China. *Int. J. Digit. Earth* **2023**, *16*, 1094–1107. [[CrossRef](#)]

17. Huang, W.; Lyu, H.; Zhang, P.; Li, H. Determination of snowmelt infiltration coefficients for seasonally frozen regions requires considering the response of the groundwater table to the freeze–thaw process. *J. Hydrol.* **2024**, *631*, 130699. [[CrossRef](#)]
18. Sun, L.Y.; Cai, Q.G.; Chen, S.Y.; He, J.J. Integrated governing system on soil and water loss of small watersheds in a typical black soil region of Northeast China. *Res. Soil Water Conserv.* **2012**, *19*, 36–41+57. (In Chinese)
19. Engman, E.T. Roughness coefficients for routing surface runoff. *J. Irrig. Drain. Eng. ASCE* **1986**, *112*, 39–53. [[CrossRef](#)]
20. Gilley, J.E.; Kottwitz, E.R.; Wieman, G.A. Darcy–Weisbach roughness coefficients for selected residue materials. *Am. Soc. Civ. Eng.* **2015**, *117*, 503–514.
21. Qi, Z.J.; Zhang, Z.X.; Yang, A.Z. Characteristics of soil erosion by water under different soil and water conservation measures on sloping farmland of black soils. *Bull. Soil Water Conserv.* **2012**, *32*, 89–92+97. (In Chinese)
22. Zhao, Y.S.; Wei, Y.X. Infiltration regularity and its simulation in the west semiarid region Heilongjiang province. *J. Irrig. Drain.* **2008**, *4*, 110–112. (In Chinese)
23. Laboratory Unse. *USDA-Water Erosion Prediction Project Hillslope Profile and Watershed Model Documentation*; NSERL Report: West Lafayette, Indiana, 1995.
24. Chen, Z.M.; Wang, B. Paths of soil erosion controlled by typical soil and water conservation practices based on the SIMWE model: A case study of the Tongshuang watershed. *Chin. J. Appl. Ecol.* **2022**, *33*, 703–710. (In Chinese)
25. Julien, P.Y.; Saghafian, B.; Ogden, F.L. Raster-based hydrologic modeling of spatially-varied surface runoff. *Water Resour.* **1995**, *31*, 523–536.
26. Mitsova, L.; Mitsova, H. Distributed soil erosion simulation for effective erosion prevention. *Water Resour. Res.* **1998**, *34*, 505–516. [[CrossRef](#)]
27. Borselli, L.; Cassi, P.; Torri, D. Prolegomena to sediment and flow connectivity in the landscape: A GIS and field numerical assessment. *Catena* **2008**, *75*, 268–277. [[CrossRef](#)]
28. Cavalli, M.; Trevisani, S.; Comiti, F.; Marchi, L. Geomorphometric assessment of spatial sediment connectivity in small Alpine catchments. *Geomorphology* **2013**, *188*, 18831–18841. [[CrossRef](#)]
29. Zandrea, F.; Michel, P.G.; Kobiyama, M. Impedance influence on the index of sediment connectivity in a forested mountainous catchment. *Geomorphology* **2019**, *351*, 106962. [[CrossRef](#)]
30. Xie, C.; Cui, B.; Xie, T.; Yu, S.L.; Liu, Z.Z.; Chen, C.; Ning, Z.H.; Wang, Q.; Zou, Y.X.; Shao, X.J. Hydrological connectivity dynamics of tidal flat systems impacted by severe reclamation in the Yellow River Delta. *Sci. Total Environ.* **2020**, *739*, 139860. [[CrossRef](#)]
31. Zandrea, F.; Michel, G.P.; Kobiyama, M.; Cardozo, G.L. Evaluation of different DTMs in the sediment connectivity determination in the Mascarada River Watershed, southern Brazil. *Geomorphology* **2019**, *332*, 80–87. [[CrossRef](#)]
32. Kang, Z.W.; Li, Y.; Huang, Z.G. Effects of DEM resolution on hydrological connectivity index of small watershed in intensive sugarcane area. *Bull. Soil Water Conserv.* **2022**, *42*, 198–207. (In Chinese)
33. Nagendra, H.; Rocchini, D. High resolution satellite imagery for tropical biodiversity studies: The devil is in the detail. *Biodivers. Conserv.* **2008**, *17*, 3431–3442. [[CrossRef](#)]
34. Vaze, J.; Teng, J.; Spencer, G. Impact of DEM accuracy and resolution on topographic indices. *Environ. Model. Softw.* **2010**, *25*, 1086–1098. [[CrossRef](#)]
35. Yan, Y.C.; Zhang, S.W.; Yue, S.P. Scale analysis of topographic factor in erosion modeling in black soil area of Northeast China. *J. Arid. Land Resour. Environ.* **2008**, *11*, 180–184. (In Chinese)
36. Gu, Z.J.; Li, A. Effects of DEM Accuracy on Soil Erosion Assessment. *J. Xinyang Norm. Univ.* **2020**, *33*, 398–404.
37. Lan, J.J.; Yu, H.Y.; Chen, L.; Ma, H.H.; Zhang, H.Y. Scale effect of airborne LiDAR DEM in watershed hydrological analysis and simulation. *Bull. Surv. Mapp.* **2020**, *4*, 40–46. (In Chinese)
38. Li, H.; Yang, W.; Liu, X.B.; Wang, Y.X.; Zhang, X.Y. Data obtained method and application for topographic threshold theory calculation of gully initiation. *Trans. Chin. Soc. Agric. Eng. (Trans. CSAE)* **2019**, *35*, 127–133. (In Chinese)
39. Zeng, B.R.; Li, Y.L.; Tan, Z.Q. Influential Factors and Environment Effects of Hydrological Connectivity in the Poyang Lake Catchment. *Resour. Environ. Yangtze Basin* **2022**, *31*, 2718–2728. (In Chinese)

Disclaimer/Publisher’s Note: The statements, opinions and data contained in all publications are solely those of the individual author(s) and contributor(s) and not of MDPI and/or the editor(s). MDPI and/or the editor(s) disclaim responsibility for any injury to people or property resulting from any ideas, methods, instructions or products referred to in the content.